Clinical Biomechanics 106 (2023) 105989

Contents lists available at ScienceDirect

Clinical Biomechanics

journal homepage: www.elsevier.com/locate/clinbiomech

Characterisation of human posterior rectus sheath reveals mechanical and structural anisotropy

Thomas Whitehead-Clarke [a,*], Christopher Brown [b], Geetika Ail [c], Vivek Mudera [d], Claire Smith [c], Alvena Kureshi [d]

[a] Centre for 3D Models of Health and Disease, Division of Surgery and Interventional Science, University College London, UK
[b] Materials Physics Group, University of Sussex, UK
[c] Department of Anatomy, Brighton and Sussex Medical School, UK
[d] Division of Surgery and Interventional Science, University College London, UK

ARTICLE INFO

Keywords:
Posterior sheath
Rectus sheath
Tensile strength
Collagen
Hernia

ABSTRACT

Background: Our work aims to investigate the mechanical properties of the human posterior rectus sheath in terms of its ultimate tensile stress, stiffness, thickness and anisotropy. It also aims to assess the collagen fibre organisation of the posterior rectus sheath using Second-Harmonic Generation microscopy.
Methods: For mechanical analysis, twenty-five fresh-frozen samples of posterior rectus sheath were taken from six different cadaveric donors. They underwent uniaxial tensile stress testing until rupture either in the transverse ($n = 15$) or longitudinal ($n = 10$) plane. The thickness of each sample was also recorded using digital callipers. On a separate occasion, ten posterior rectus sheath samples and three anterior rectus sheath samples underwent microscopy and photography to assess collagen fibre organisation.
Findings: samples had a mean ultimate tensile stress of 7.7 MPa (SD 4.9) in the transverse plane and 1.2 MPa (SD 0.8) in the longitudinal plane ($P < 0.01$). The same samples had a mean Youngs modulus of 11.1 MPa (SD 5.0) in the transverse plane and 1.7 MPa (SD 1.3) in the longitudinal plane ($P < 0.01$). The mean thickness of the posterior rectus sheath was 0.51 mm (SD 0.13). Transversely aligned collagen fibres could be identified within the posterior sheath tissue using Second-Harmonic Generation microscopy.
Interpretation: The posterior rectus sheath displays mechanical and structural anisotropy with greater tensile stress and stiffness in the transverse plane compared to the longitudinal plane. The mean thickness of this layer is around 0.51 mm – consistent with other studies. The tissue is constructed of transversely aligned collagen fibres that are visible using Second-Harmonic Generation microscopy.

1. Introduction

The anatomy of muscular and fascial layers of the abdominal wall has been well-understood for many years. Less well understood however are the mechanical properties of each layer, and how that may relate to the microscopic collagen structure of each layer. One of the lesser investigated structures is the posterior rectus sheath (PRS). Whilst a number of studies have examined the mechanical properties of either the linea alba and/or anterior rectus sheath (Ben Abdelounis et al., 2013; Cooney et al., 2016; Forstemann et al., 2011; Grassel et al., 2005; Levillain et al., 2016; Martins et al., 2012), the mechanical properties of the PRS have been analysed only three times in the literature (Astruc et al., 2018; Hollinsky and Sandberg, 2007; Rath et al., 1997). The linea alba is the most frequently studied tissue within the anterior abdominal wall (Deeken and Lake, 2017) – likely due to the prevalence of midline ventral hernias. Two articles by Axer et al. (Axer et al., 2001a; Axer et al., 2001b) explore the collagen microstructure of the PRS as well as other layers in the abdominal wall.

As techniques within hernia surgery have evolved, the PRS has become increasingly important to understand for the purposes of repair. Increasingly, large ventral hernias are repaired using a "Reeves-Stoppa" repair where the PRS is dissected away from the rectus muscles, fascia closed and then a mesh placed in the retro-rectus space (Stoppa et al., 1987). Some have suggested this technique may reduce post-operative infections and recurrence (Holihan et al., 2016; Timmermans et al., 2014). Newer techniques such as the Transversus Abdominus Release

* Corresponding author at: Centre for 3D Models of Health and Disease, Division of Surgery and Interventional Science, University College London, UK.
E-mail address: rmhktiw@ucl.ac.uk (T. Whitehead-Clarke).

https://doi.org/10.1016/j.clinbiomech.2023.105989
Received 4 January 2023; Accepted 10 May 2023
Available online 18 May 2023

Fig. 1. A 'dog bone' shaped section of human posterior rectus sheath before uniaxial tensile strength testing.

Table 1
Summary of mean values for UTS and modulus from each donor.

Donor	Mean UTS (MPa)		Mean Modulus (MPa)	
	Transverse	Longitudinal	Transverse	Longitudinal
A	4.81	0.94	11.097	1.459
B	11.86	0.94	11.710	0.845
C	11.63	1.69	12.974	2.586
D	3.15	0.13	5.702	0.164
E	7.92	1.45	11.075	1.996
F	7.48	N/A	13.305	N/A

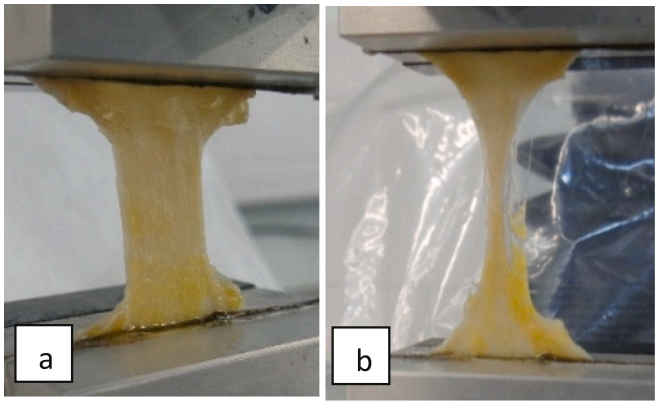

Fig. 2. a + b: *(a)* A dog bone shaped sample of PRS within the clamps of mechanical testing equipment. *(b)* A tissue sample mid-way through testing, rupturing at the centre of the test sample.

(TAR) are also growing in popularity (Krpata et al., 2013) which involve a division of the Transversus Abdominus muscle to facilitate midline closure. Due to this increased relevance of the PRS within the field of hernia surgery, it is prudent that we develop a better understanding of its mechanical and structural properties.

The collagen structure of weight bearing tissues can be a key indicator of their mechanical properties – for example the uniform alignment of the Achilles tendon vs the multidirectional organisation of skin collagen (Lin et al., 2020). As such, understanding the organisation of collagen fibres in the PRS is useful to better understand not only its mechanical properties, but what normal "healthy" tissue looks like (Hollinsky and Sandberg, 2007). Our work looks to add to the current knowledge about this fascial layer and explore the use of Second-Harmonic Generation (SHG) microscopy – not previously used to

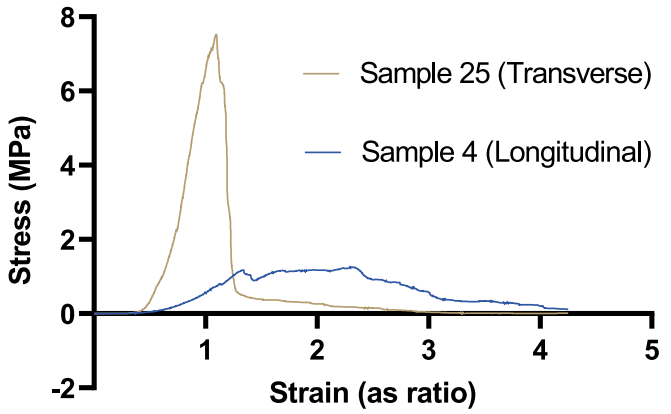

Fig. 3. Representative stress/ strain graphs for "typical" transverse and longitudinal PRS samples. Each sample has been selected for this graph as its UTS value represents the median value for its group.

image the PRS. Better understanding of this tissue's structural and mechanical characteristics will help groups such as ours in developing 3D tissue models capable of better understanding rectus sheath healing, and potential herniation. This work, therefore, set out to measure the uniaxial tensile strength of the PRS in both transverse and longitudinal directions as well as analyse its collagen structure using second harmonic generation microscopy.

2. Materials and methods

2.1. Tissue sampling

Permission was granted by the Designated Individual at Brighton and Sussex Medical School (Human Tissue Authority licence for Anatomical Examination 12,098). Donors consented to this scheduled purpose and sections of rectus sheath tissue for the purposes of this study. All donors provided consent for image retention. Due to the logistics and techniques required, the study was carried out over two discrete occasions – each after donor cadavers had been used for educational courses. On the first occasion, tissue was sampled for mechanical analysis and testing of tissue thickness. On the second occasion, tissue was taken for the purposes of microscopic analysis.

2.1.1. For mechanical testing

Twenty-five different PRS samples were taken from six separate cadavers (details of cadavers and sample numbers can be found in appendix 1). All donor cadavers were 'fresh-frozen' rather than embalmed and had been thawed at room temperature after being frozen at -20 °C. Cadavers began thawing eight days before tissue sampling, and eleven days before mechanical testing. The entire PRS (excluding parietal peritoneum) was dissected out, and dog bone shapes of tissue were cut out from the PRS (Fig. 1). Samples were only used from tissue above the umbilicus. Samples were cut out in a mixture of transverse ($n = 15$) and longitudinal ($n = 10$) directions (respective to cadaveric anatomy). The number of samples used for each direction was determined by establishing the optimal way to maximise the total sample number. PRS testing samples were cut to shape as per Hollinsky et al. (Hollinsky and Sandberg, 2007) briefly, samples were cut to 'dog bone' shapes with a testing width of 10 mm, and a maximum length of 30 mm. These shapes were produced by cutting around a 3D-printed dog-bone shaped stencil with a surgical scalpel. Such shapes are important to ensure that rupture of the samples occurs centrally – often cited within ASTM guidance (ASTM, 2023). Samples were then placed in a folded gauze soaked with Phosphate Buffered Saline (PBS), placed between two pieces of cardboard in order to be kept flat, then wrapped in cling film to prevent drying out. Samples were then refrigerated at 4 °C for 72 h until testing.

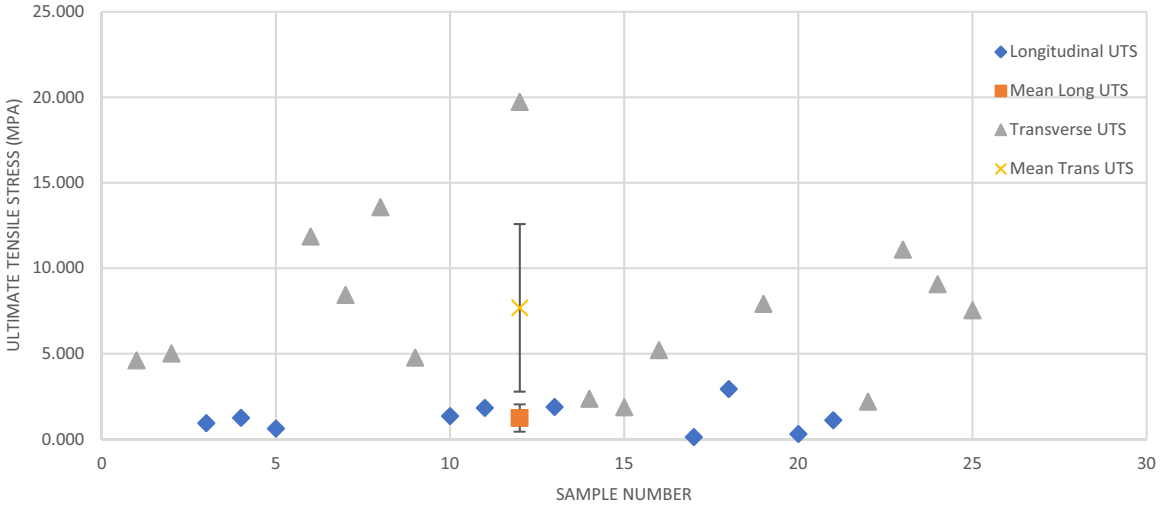

Fig. 4. A graph showing the UTS of 25 different PRS samples with mean (SD) of both transverse ($n = 15$) and longitudinal ($n = 10$) groups.

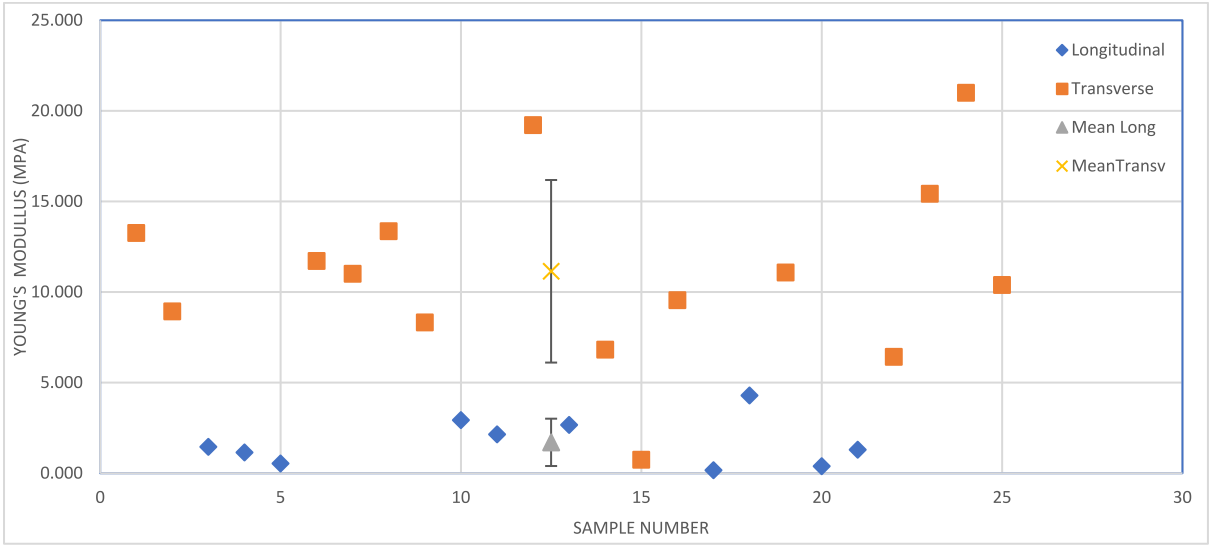

Fig. 5. A graph showing the Young's Modulus of 25 different PRS samples and the mean (SD) of longitudinal (n = 10) and transverse (n = 15) groups.

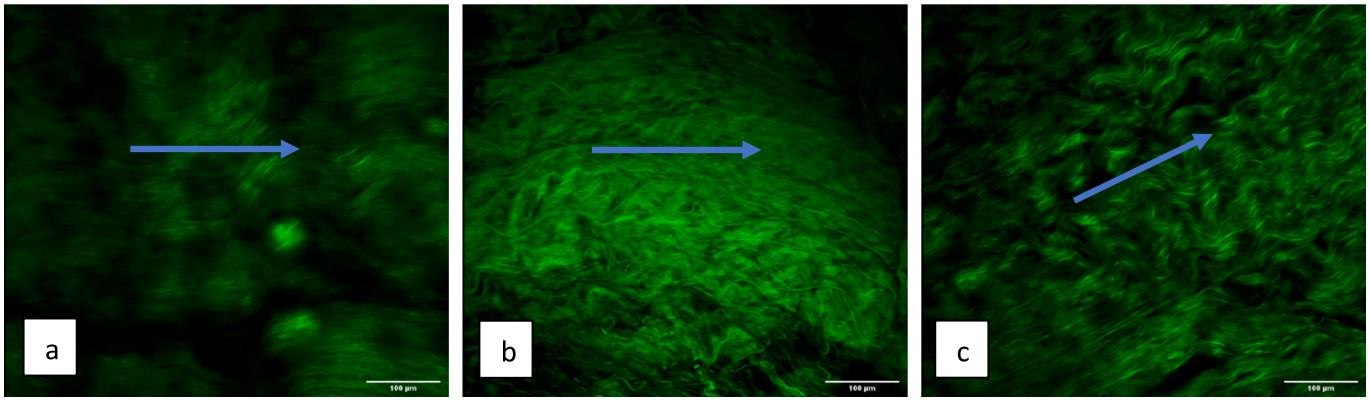

Fig. 6. a,b,c: SHG images from PRS samples from three different cadaveric donors. All exhibit well organised collagen fibres – most aligned in a transverse direction. Scale bar - 100 μm.

2.1.2. For microscopy

Two samples of PRS were taken from each of five different cadaveric donors (one left sided, one right sided). Two samples of anterior rectus sheath were also taken from one donor as a comparison/ control. Donor cadavers had been frozen as per the mechanical testing samples. Cadavers were thawed at room temperature for seven days before tissue

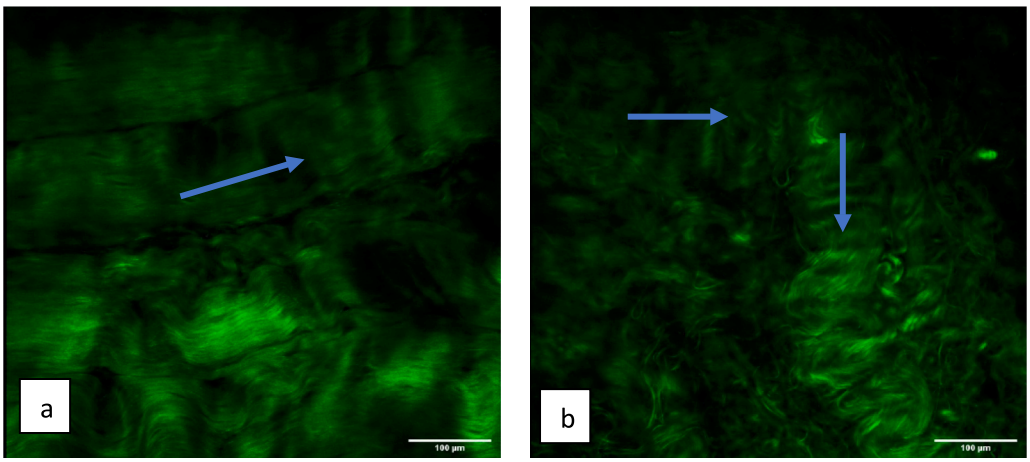

Fig. 7. a + b – Images of 2 Anterior Rectus Sheath samples – on the left (a) organised and aligned collagen fibres can be seen. On the right (B) some fibres can be seen running perpendicular to each other. Scale bar 100 μm.

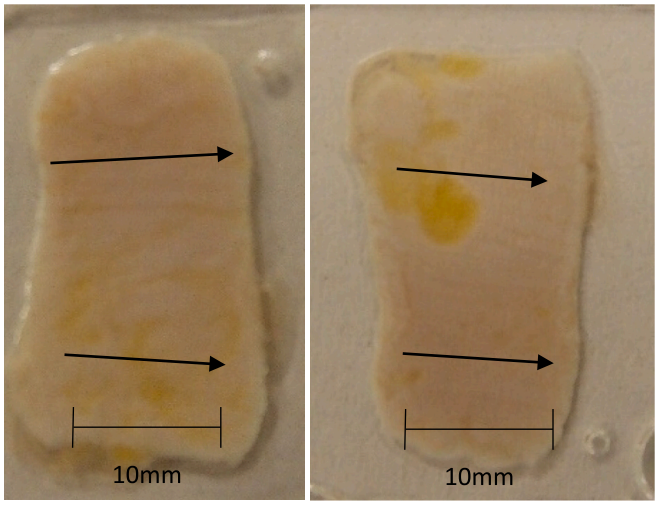

Fig. 8. a + b: *Posterior rectus sheath* - both images taken of the same sample – turned on its transverse axis. Fibres run transversely on either side. Scale bars are approximate.

sampling, and ten days before microscopy. Samples were only taken from above the umbilicus. Samples were washed with PBS and then placed on microscope slides so as to maintain their anatomical orientation. Samples were mounted under cover slips using histomount solution *(Life technologies Frederick USA),* left to dry, and then underwent microscopy three days later.

2.2. Mechanical testing and assessment of thickness

When samples were ready for use, they were removed from refrigeration and kept in their PBS-soaked gauze at room temperature before use. All samples were tested within the same five-hour period. Immediately before mechanical testing, samples were removed from their gauze wrapping and placed within the grips of the tensile strength testing apparatus. Tissue samples were tested using a TA XT + Texture Analyser – with 50 kg (~ 0.5 kN) loadcell (Stable Micro Systems, Godalming, Surrey, UK). Samples were placed between clamps that had been lined with sandpaper for maximum grip. Once in position, a single measurement was taken using digital callipers at the centre point of the sample to measure tissue thickness. The individual operating the callipers was blinded to measurement. Tissue samples were then pulled apart at 10 mm/min until sample rupture. Data output was stored by Stable Micro Systems 'Exponent' software which recorded the stress, σ, as a function of tensile strain, ε, of each sample. In this study, we have measured the normal linear tensile stress, a scalar quantity and special case of the Cauchy stress, where the force applied is assumed to be

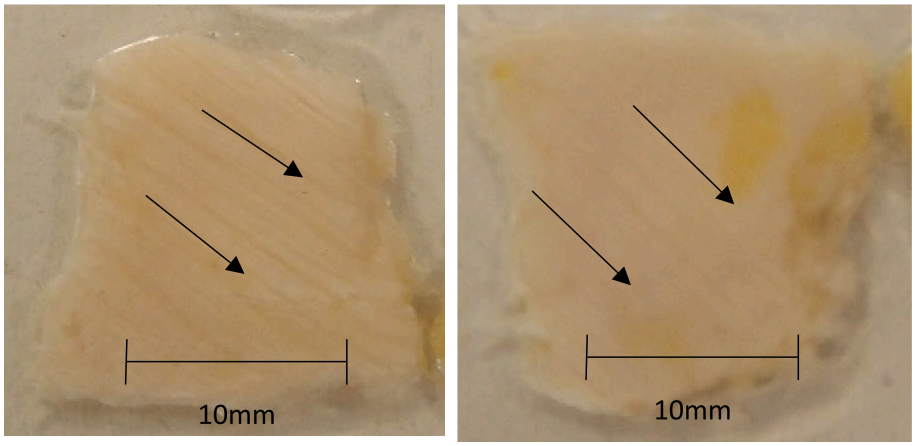

Fig. 9. a + b*: Anterior rectus sheath* –both images taken of the same sample turned over on its transverse axis. Oblique fibres run in the same direction on either side. Scale bars are approximate.

always parallel to the normal of the stress area, with no shear stress present. This assumption is consistent with the experimental setup and observations of the samples during testing. From the output stress/strain curves, both tensile Young's modulus, Y, and Ultimate tensile stress (UTS), σ_{max}, were computed.

2.3. Second-harmonic generation (SHG) microscopy

Tissue samples were mounted on standard microscope slides underneath cover slips – mounted using Histomount solution. Individual images of a single z-depth were taken using a Bergamo II Multiphoton microscope (Thor Labs New Jersey, USA) equipped with a 20× Olympus XLUMPLFLN 20×/1.0 W water immersion lens (Olympus, Hamburg, Germany) and powered by a Chameleon Vision II Laser (Coherent, California USA). SHG images were taken using an excitation frequency of 850 nm. Files were saved in ".tiff" format then converted to .jpg format using Zeiss zen blue software (Zeiss, Oberkochen Germany).

2.4. Photography

Digital photographs of the front and rear of samples were taken using a Nikon Coolpix L810 digital camera (Nikon, Tokyo, Japan).

2.5. Data and statistical analysis

Data from mechanical testing was analysed using Python 3.8 using the Zeus MCMC Ensemble Slice Sampler package (Karamanis et al., 2021; Karamanis and Beutler, 2021). The ensemble slice sampler was used to identify the most linear region of each sample's stress-strain curve, by determining the region of data with the lowest chi-squared value, i.e. best possible fitting region, as compared to a linear model. The modulus value was taken from this computationally determined best-fitting linear region, which was typically between strain values of 40% to 70%. This method helped avoid risk of experimental uncertainties from poor fitting across any partial sample fracture. From this linear region, tensile Young's modulus values were computed as the gradient of a linear fit to the data, $Y = d\sigma/d\varepsilon$, as well as associated uncertainties. These values were combined to find a numerical mean value of Y for each of longitudinal and transverse tissue types, as well as associated statistical standard deviations.

The peak stress of each stress-strain curve was also identified computationally, which defined the UTS of the sample. These values were combined to find a numerical mean value of UTS (σ_{max})for each of longitudinal and transverse tissue types, as well as associated statistical standard deviations.

The statistical significance of both the UTS and Youngs Modulus between each group (Transverse Vs Longitudinal) was calculated using a Mann-Whitney test. To adjust for multiple samples being taken from the same cadaveric donor (and therefore not biologically independent), mean values were calculated for both modulus and UTS for all similarly orientated samples taken from each donor. The subsequent Mann-Whitney test was performed using SPSS (version 29.0, IBM 2022).

3. Results

3.1. Thickness of rectus sheath

One single measurement was taken for each of the samples. Measurements ranged from 0.24 mm to 0.67 mm. The mean thickness was 0.51 mm (SD 0.13).

3.2. Mechanical properties

All samples failed structurally within the length of the 10 mm wide centre of the "dog bone" test sample. Overall, transverse oriented samples were found to have a greater UTS and Youngs Modulus than longitudinal samples. Fig. 3 provides a representative stress-strain curve for each group showing a higher and steeper curve for the transverse sample. This graph was developed by using the entire stress/strain curve for one representative sample from each group. Samples (numbered 4 and 25) were selected as their UTS values were the median value for their group.

Focusing on the mean values for each group, there was a statistically significant difference in both the UTS and Young's modulus between longitudinal and transverse groups. Figs. 4 and 5 show UTS and modulus values respectively for all samples as well as their mean and standard deviation. Transverse orientated samples had a mean UTS of 7.7 MPa (SD 4.9) whereas Longitudinal samples had a mean UTS of 1.2 MPa (SD 0.8) ($p < 0.01$). Transverse samples had a mean Youngs modulus of 11.1 MPa (SD 5.0) whereas Longitudinal samples had a mean Youngs Modulus of 1.7 MPa (SD 1.3) ($P < 0.01$). Table 1 provides a summary of the mean values calculated for similarly oriented samples from each cadaveric donor for the purposes of statistical analysis.

3.3. Second harmonic generation microscopy

Ten tissue samples underwent microscopy (two each from five cadavers, one right sided and one left sided). An additional three samples of anterior sheath were taken from one cadaver for comparison. Reliable collagen images could not be obtained from four of the PRS samples – due likely to tissue decomposition. All PRS samples showed highly aligned and organised collagen fibres. Most fibres were orientated in a transverse direction (Fig. 6a,b,c). Several images were also taken of anterior sheath samples, where again, highly aligned and organised collagen fibres could be seen (Fig. 7a). Some samples displayed the presence of perpendicular fibres (Fig. 7b) as per Axer at al (Axer et al., 2001a). All images of both the anterior and posterior rectus sheath exhibit a wave-like structure of the collagen fibres – known as 'crimp'. This structure has been well discussed in fibre-forming collagens (Gathercole and Keller, 1991) and displayed in the posterior rectus sheath previously (Axer et al., 2001a).

3.4. Photography

Upon inspection, collagen bundles within the tissue were visible to the naked eye. As a result, photographs were taken to demonstrate their relative orientation. Fig. 8a and b clearly display the two opposing sides of the PRS (the same sample is flipped 180^{o} on its horizontal axis). Horizontal/ transverse collagen bundles are clearly visible within the tissue that remain similarly oriented on either side. Similar images (Fig. 9a+b) were taken from the same sample of anterior rectus sheath flipped on its horizontal axis. Collagen bundles are clearly visible in the same direction on both images – indicating that there are bundles running in perpendicular directions within the tissue as previously described by Axer et al. (Axer et al., 2001a).

4. Discussion

Our work is one of few studies analysing the uniaxial tensile strength of the PRS and is the first to correlate its mechanical strength with its structural anisotropy. It is also only the second study to conduct PRS mechanical testing in a more accurate manner using 'dog bone' tissue samples (Hollinsky and Sandberg, 2007) and the second to study the Young's Modulus of the PRS (Astruc et al., 2018).

As our group previously identified with fascia/ mesh mechanical testing (Whitehead-Clarke et al., 2021), techniques used across the literature can vary greatly. In order, therefore, to establish consistency, methods including testing speed (10 mm/min) and tissue shape/size were adopted from one of the largest studies in the literature by Hollinsky et al. (Hollinsky and Sandberg, 2007). Hollinsky's study arrived at values similar to ours; a mean UTS of 5.6 MPa (7.7 in our study) in the transverse plane and 1.9 MPa (1.2 in our study) in the longitudinal

plane. Whilst Hollinsky et al. did not publish their PRS thickness values, our study established a mean thickness of 0.51 mm (SD 0.13) – a measurement relatively consistent with figures from other large studies (Axer et al., 2001a) (between 0.4 and 0.5 mm).

Another similarity between Hollinsky's work and ours is the large standard deviation for both transverse and longitudinal UTS values (Hollinsky and Sandberg, 2007) – something with a number of potential causes. Firstly, digital calliper measurement of sample thickness may lack the sensitivity when measuring such thin samples (<1 mm). With such fine margins, inaccurate measurements could greatly affect UTS calculations when given in MPa (N/mm^2). Whilst other potentially more accurate methods have been described (Astruc et al., 2018), any method that involves compression of the tissue potentially compromises not only accuracy but also tissue integrity. Another factor likely to contribute to variance in strength is the fibrillar nature of the rectus sheath. The rectus sheath is not a uniform plastic structure, and therefore naturally contains areas of variation. The fibrous structure can be seen in Fig. 2b, with strands breaking at different rates. This lack of a uniform structure will obviously lead to varied strength across the tissue. Finally, samples from our study were taken from individuals of varied age and weight (see appendix 1) as well as other health and lifestyle factors. These factors may affect structural integrity of tissue samples - causing variation across measurements.

We believe that understanding the mechanical properties of abdominal fascia is an important area in the field of hernia surgery that has thus far been undervalued. Firstly, for the development of new synthetic biomaterials (mesh) for hernia repair, products would be best designed with a mechanical strength, stiffness and anisotropy that matched tissues being repaired. Increasingly for large ventral hernias, meshes are placed over the PRS in the "retro-rectus" plane (Holihan et al., 2016). As such, understanding this layer's strength and anisotropy will help to develop ideal biomaterials for repair. In addition, the study of herniation and repair has evolved in recent years to embrace computational modelling of the abdominal wall (Qandeel et al., 2022; Todros et al., 2018). Such research benefits greatly from real-world measurements of the mechanical properties of each fascial layer. Greater amounts of data in the literature concerning these mechanical properties will lead to more accurate computational models.

The collagen structure of load-bearing tissues is often related to the purpose of that tissue (Silver et al., 2003). One example of this is the uniformly aligned fibres with the Achilles tendon (a tissue under significant unidirectional stress), compared to the randomly aligned fibres with human skin – which are under stress from a number of different directions (Lin et al., 2020). It is not surprising therefore that both our work and that by Axer et al. (Axer et al., 2001a) concluded that fibres in the posterior sheath are orientated transversely. Such directionality is likely a remnant of their relation to the transversus abdominus muscle. A similar pattern has also been observed in our group's work on the transversalis fascia (Kureshi et al., 2008).

During our study, we were also able to obtain macroscopic and microscopic images of both the posterior and anterior rectus sheath using photography and SHG respectively. In their study, Axer et al. discuss the perpendicular "criss-cross" nature of fibres within the anterior rectus sheath (Axer et al., 2001a). Whilst not a key purpose of our work, Fig. 9a and b clearly show oblique collagen fibres that do not change orientation despite the sample being 'flipped' 180 degrees. This suggests that fibres on the back run perpendicular to those on the front. Whether or not these fibres form two distinct layers or whether there is an intermingling of fibres as per Axer et al. (Axer et al., 2001a) {Axer, 2001 #1659} is yet to be established. SHG images in Fig. 8b were able to demonstrate some fibres running perpendicular to each another. All images demonstrated a 'crimp' pattern within the collagen fibres that has been previously exhibited in the posterior sheath (Axer et al., 2001a) as well as other fibre-forming collagen structures (Gathercole and Keller, 1991). Whilst some have explored the effect of strain upon the microscopic appearance of linea alba tissue (Levillain et al., 2016), the effect that strain has upon 'crimp' structure (as seen in mouse tail tendons by Legerlotz et al. (Legerlotz et al., 2014)) would be a novel observation in abdominal fascia.

By establishing this new technique of imaging human rectus sheath using SHG microscopy, we hope that others will make optimal use of this technology to obtain in-depth understanding of collagen alignment both in healthy and diseased tissue. Work such as that by Hollinsky et al. that reviewed the strength of scar tissue in the abdominal wall (Hollinsky and Sandberg, 2007), could benefit from SHG imaging to establish the relationship between collagen structure and mechanical strength.

Our work is of course not without its limitations. Firstly, given that tissues underwent mechanical testing more than ten days after thawing, it is possible that the strength of the PRS may be compromised by decomposition. In addition, thickness measurements of the PRS may be rendered inaccurate due to the sensitivity of digital callipers and their ability to press into tissue when closed fully. Others have, however, reviewed non-contact methods such as laser displacement sensors – finding them less accurate than simple callipers (O'Leary et al., 2013).

Samples in our study were stripped of peritoneum but could not be safely stripped of transversalis fascia without potential damage to the PRS. As such, samples assessed were constituted of both PRS and transversalis fascia. Whilst this may render our values not exclusively applicable to the PRS, the transversalis fascia and PRS are, for practical purposes of abdominal wall closure – the same layer. Other studies in this area have similarly not described separation of transversalis fascia and PRS (Hollinsky and Sandberg, 2007).

Whilst a uniaxial analysis is the most commonly performed method for tensile strength testing, useful additions to our work would include both biaxial and "ball burst" testing of the same tissue. Such testing methods are more physiologically relevant tests for the rectus sheath which is exposed to multi-directional forces. Clearly a larger data set involving a greater number of cadavers would provide a more robust data set. Such work may also look to explore the effects of age, sample site and BMI upon mechanical properties.

In summary, we present one of the few studies of its kind to explore the mechanical and structural properties of the posterior rectus sheath. This study has evidenced both the structural and mechanical anisotropy of the tissue and explored a novel technique for imaging (SHG microscopy). Further studies comparing healthy Vs hernia tissue in this way may be informative to better understand the pathophysiology of herniation.

Declaration of Competing Interest

The authors declare the following financial interests/personal relationships which may be considered as potential competing interests:

Thomas Whitehead-Clarke reports financial support was provided by The British Hernia Society.

Acknowledgements

This work was supported financially by research grants from the British Hernia Society.

We would like to thank Professor Claire Smith and Camilla Ingram from the Department of Anatomy at Brighton and Sussex Medical School. We would also like to thank Dr. Alice King from the Materials Physics Group at the University of Sussex, as well as Yan Gu from the Wolfson Centre for Medical Imaging at University of Sussex.

Appendix A. Supplementary data

Supplementary data to this article can be found online at https://doi.org/10.1016/j.clinbiomech.2023.105989.

References

ASTM, 2023. Standard Test Method for Tensile Properties of Plastics1. https://doi.org/10.1520/d0638-14.

Astruc, L., De Meulaere, M., Witz, J.-F., Nováček, V., Turquier, F., Hoc, T., Brieu, M., 2018. Characterization of the anisotropic mechanical behavior of human abdominal wall connective tissues. J. Mech. Behav. Biomed. Mater. 82, 45–50. https://doi.org/10.1016/j.jmbbm.2018.03.012.

Axer, H., Keyserlingk, D.G., Prescher, A., 2001a. Collagen fibers in linea alba and rectus sheaths. I. General scheme and morphological aspects. J. Surg. Res. 96 (1), 127–134. https://doi.org/10.1006/jsre.2000.6070.

Axer, H., Keyserlingk, D.G.V., Prescher, A., 2001b. Collagen fibers in Linea Alba and rectus sheaths: II. Variability and biomechanical aspects. J. Surg. Res. 96 (2), 239–245. https://doi.org/10.1006/jsre.2000.6071.

Ben Abdelounis, H., Nicolle, S., Otténio, M., Beillas, P., Mitton, D., 2013. Effect of two loading rates on the elasticity of the human anterior rectus sheath. J. Mech. Behav. Biomed. Mater. 20, 1–5. https://doi.org/10.1016/j.jmbbm.2012.12.002.

Cooney, G.M., Lake, S.P., Thompson, D.M., Castile, R.M., Winter, D.C., Simms, C.K., 2016. Uniaxial and biaxial tensile stress-stretch response of human linea alba. J. Mech. Behav. Biomed. Mater. 63, 134–140. https://doi.org/10.1016/j.jmbbm.2016.06.015.

Deeken, C.R., Lake, S.P., 2017. Mechanical properties of the abdominal wall and biomaterials utilized for hernia repair. J. Mech. Behav. Biomed. Mater. 74, 411–427. https://doi.org/10.1016/j.jmbbm.2017.05.008.

Forstemann, T., Trzewik, J., Holste, J., Batke, B., Konerding, M.A., Wolloscheck, T., Hartung, C., 2011. Forces and deformations of the abdominal wall–a mechanical and geometrical approach to the linea alba. J. Biomech. 44 (4), 600–606. https://doi.org/10.1016/j.jbiomech.2010.11.021.

Gathercole, L.J., Keller, A., 1991. Crimp morphology in the fibre-forming collagens. Matrix 11 (3), 214–234. https://doi.org/10.1016/S0934-8832(11)80161-7.

Grassel, D., Prescher, A., Fitzek, S., Keyserlingk, D.G., Axer, H., 2005. Anisotropy of human linea alba: a biomechanical study. J. Surg. Res. 124 (1), 118–125. https://doi.org/10.1016/j.jss.2004.10.010.

Holihan, J.L., Nguyen, D.H., Nguyen, M.T., Mo, J., Kao, L.S., Liang, M.K., 2016. Mesh location in open ventral hernia repair: a systematic review and network Meta-analysis. World J. Surg. 40 (1), 89–99. https://doi.org/10.1007/s00268-015-3252-9.

Hollinsky, C., Sandberg, S., 2007. Measurement of the tensile strength of the ventral abdominal wall in comparison with scar tissue. Clin. Biomech. 22 (1), 88–92. https://doi.org/10.1016/j.clinbiomech.2006.06.002.

Karamanis, M., Beutler, F., 2021. Ensemble slice sampling. Stat. Comput. 31 (5), 61. https://doi.org/10.1007/s11222-021-10038-2.

Karamanis, M., Beutler, F., Peacock, J.A., 2021. Zeus: A Python Implementation of Ensemble Slice Sampling for Efficient Bayesian Parameter Inference. Monthly Notices of the Royal Astronomical Society.

Krpata, D.M., Stein, S.L., Eston, M., Ermlich, B., Blatnik, J.A., Novitsky, Y.W., Rosen, M. J., 2013. Outcomes of simultaneous large complex abdominal wall reconstruction and enterocutaneous fistula takedown. Am. J. Surg. 205 (3), 354–358 discussion 358-359. https://doi.org/10.1016/j.amjsurg.2012.10.013. discussion 358-359.

Kureshi, A., Vaiude, P., Nazhat, S.N., Petrie, A., Brown, R.A., 2008. Matrix mechanical properties of transversalis fascia in inguinal herniation as a model for tissue expansion. J. Biomech. 41 (16), 3462–3468. https://doi.org/10.1016/j.jbiomech.2008.08.018.

Legerlotz, K., Dorn, J., Richter, J., Rausch, M., Leupin, O., 2014. Age-dependent regulation of tendon crimp structure, cell length and gap width with strain. Acta Biomater. 10 (10), 4447–4455. https://doi.org/10.1016/j.actbio.2014.05.029.

Levillain, A., Orhant, M., Turquier, F., Hoc, T., 2016. Contribution of collagen and elastin fibers to the mechanical behavior of an abdominal connective tissue. J. Mech. Behav. Biomed. Mater. 61, 308–317. https://doi.org/10.1016/j.jmbbm.2016.04.006.

Lin, J., Shi, Y., Men, Y., Wang, X., Ye, J., Zhang, C., 2020. Mechanical roles in formation of oriented collagen fibers. Tissue Eng. Part B Rev. 26 (2), 116–128. https://doi.org/10.1089/ten.TEB.2019.0243.

Martins, P., Peña, E., Jorge, R.M.N., Santos, A., Santos, L., Mascarenhas, T., Calvo, B., 2012. Mechanical characterization and constitutive modelling of the damage process in rectus sheath. J. Mech. Behav. Biomed. Mater. 8, 111–122. https://doi.org/10.1016/j.jmbbm.2011.12.005.

O'Leary, S.A., Doyle, B.J., McGloughlin, T.M., 2013. Comparison of methods used to measure the thickness of soft tissues and their influence on the evaluation of tensile stress. J. Biomech. 46 (11), 1955–1960. https://doi.org/10.1016/j.jbiomech.2013.05.003.

Qandeel, H., Chew, C., Tanner, K.E., O'Dwyer, P.J., 2022. Testing meshes in a computer model of a laparoscopic ventral hernia repair. Surg. Endosc. 36 (6), 4124–4128. https://doi.org/10.1007/s00464-021-08735-0.

Rath, A.M., Zhang, J., Chevrel, J.P., 1997. The sheath of the rectus abdominis muscle: an anatomical and biomechanical study. Hernia 1 (3), 139–142. https://doi.org/10.1007/BF02426420.

Silver, F.H., Freeman, J.W., Seehra, G.P., 2003. Collagen self-assembly and the development of tendon mechanical properties. J. Biomech. 36 (10), 1529–1553. https://doi.org/10.1016/s0021-9290(03)00135-0.

Stoppa, R., Louis, D., Verhaeghe, P., Henry, X., Plachot, J.P., 1987. Current surgical treatment of post-operative eventrations. Int. Surg. 72 (1), 42–44.

Timmermans, L., de Goede, B., van Dijk, S.M., Kleinrensink, G.J., Jeekel, J., Lange, J.F., 2014. Meta-analysis of sublay versus onlay mesh repair in incisional hernia surgery. Am. J. Surg. 207 (6), 980–988. https://doi.org/10.1016/j.amjsurg.2013.08.030.

Todros, S., Pachera, P., Baldan, N., Pavan, P.G., Pianigiani, S., Merigliano, S., Natali, A. N., 2018. Computational modeling of abdominal hernia laparoscopic repair with a surgical mesh. Int. J. Comput. Assist. Radiol. Surg. 13 (1), 73–81. https://doi.org/10.1007/s11548-017-1681-7.

Whitehead-Clarke, T., Karanjia, R., Banks, J., Beynon, V., Parker, S., Sanders, D., Mudera, V., Windsor, A., Kureshi, A., 2021. The experimental methodology and comparators used for in vivo hernia mesh testing: a 10-year scoping review. Hernia. https://doi.org/10.1007/s10029-020-02360-x.